

# DeepCRE: Revolutionizing Drug R&D with Cutting-Edge Computational Models

Yushuai Wu<sup>1</sup>

<sup>1</sup>Institute for AI Industry Research (AIR), Tsinghua University, Beijing, 100084, China

## Abstract

The field of pharmaceutical development and therapeutic application both face substantial challenges. Therapeutic domain calls for more treatment alternatives while numerous promising pre-clinical drugs fail in clinical trails. One of the reasons is the inadequacy of Cross-drug Response Evaluation (CRE) during the late stage of drug development. Although in-silico CRE models offer a solution to this problem, existing methodologies are either limited to early development stages or lack the capacity for a comprehensive CRE analysis. Herein, we introduce a novel computational model named DeepCRE and present the potential of DeepCRE in advancing therapeutic discovery and development. DeepCRE outperforms the existing best models by achieving an average performance improvement of 17.7% in patient-level CRE, and a 5-fold increase in indication-level CRE. Furthermore, DeepCRE has identified six drug candidates that show significantly greater effectiveness than a comparator set of two approved drug in 5/8 colorectal cancer (CRC) organoids. This highlights DeepCRE's ability to identify a collection of drug candidates with superior therapeutic effects, underscoring its potential to revolutionize the field of therapeutic development.

arXiv:2403.03768v1 [cs.AI] 6 Mar 2024

## Introduction

The field of pharmaceutical development and therapeutic application both face substantial challenges[1, 2, 3, 4]. In the realm of therapeutic application, the scarcity of effective treatment options is a critical concern for medical researchers[2]. This challenge was highlighted in a recent article in the Nature journal, entitled "The future of precision cancer therapy might be to try everything", advocating for a comprehensive exploration of treatment alternatives[1]. Unfortunately, the reality is characterized by a constricted repertoire of available drugs[2]. On the other hand, the domain of drug development confronts the phenomenon known as "Eroom's Law", which posits that, counterintuitively, the efficiency of developing new drugs is declining despite advancements in technology[5]. The failure of numerous promising pre-clinical drugs during clinical trials highlights the obstacles in expanding the spectrum of effective treatments.

A pivotal factor exacerbating these challenges is the inadequacy of Cross-drug Response Evaluation (CRE), which is essential for reducing costs and enhancing efficiency in the drug development stage[6], and for improving prognosis outcomes in the therapeutic stage[2, 7, 8]. Yet, due to technological and ethical constraints, CRE has largely been restricted to the target and cell-line level[9, 10], representing the early stage of drug development (Fig. 1a). Hopefully, Artificial Intelligence (AI) has emerged as a key technology with the potential to predict the CRE in the late stage (Fig. 1a), offering new approach to exploring treatment strategies more effectively[11, 12].

Recently, there have been some related researches [13, 14, 10, 15, 16]. Single-Drug Learning (SDL) models, such as ADAE[13] and Code-AE[14], have demonstrated potential in developing personalized treatment and identifying patient biomarkers. Nonetheless, these models fall short in the capability of comprehensive CRE, restricting their broader applications. In contrast, Multi-Drug Learning (MDL) models, including DrugCell[10], Paccmann[15] and TGSA[16], leverage extensive drug response data and facilitate cross-drug response comparisons [17]. However, MDL models are generally restricted to the cell-line level [17], which may result in suboptimal performance when predicting patient drug responses due to the disparities between cell lines and patients.

Here, we introduce DeepCRE, a novel computational model that significantly enhances CRE at the patient-level, demonstrating an average performance boost of 17.77% over existing state-of-the-art (SOTA) models[13, 14, 10, 15, 16]. Furthermore, our model shows a remarkable 5-fold improvement in indication-level CRE, outperforming all previous SOTA models. Finally, we present compelling evidence of DeepCRE's potential in drug repurposing for colorectal cancer (CRC). The model has identified a set of six drug candidates (Set A) that are significantly more effective than a comparator set of two approved drugs (Set C) in 5/8 CRC organoids testing, underscoring the potential of DeepCRE in advancing therapeutic discovery and development. To note, it is not merely about identifying one or two potential drugs, rather, it highlights the capability of DeepCRE to uncover a collection of drug candidates with enhanced therapeutic effects.

# Results

## Overview of DeepCRE

The drug research and design (R&D) process encompasses target identification, cell line assays, animal or organoid testing and clinical trials[18]. A significant number of drug candidates fail at various stages, resulting in inefficient drug development[5, 19]. Interestingly, there is a magical connection between the success rate and the CRE abundance in every stage of drug R&D, where multiple CRE exist in the early stage while few CRE remain in the late stage (Fig. 1a). Enhancing the presence of CREs in later stages, especially with the aid of in-silico CRE models, could markedly improve drug development outcomes (Fig. 1a,b).

The principle of DeepCRE is to project the cell line and patient data onto a common space, which is suitable for drug response prediction (Fig. 1c). This methodology has contributed to an average performance boost of 17.7% and a 5-fold improvement in patient and indication-level CRE prediction, respectively, surpassing existing SOTA models (Fig. 1c). Notably, DeepCRE has identified six drug candidates (Set A) that exhibit significantly higher effectiveness than two approved drugs (Set C) in 5 out of 8 CRC organoids tested (Fig. 1c-e). To note, it is not merely about identifying one or two potential drugs, rather, it highlights the capability of DeepCRE to uncover a collection of drug candidates with enhanced therapeutic effects.

## The construction of the DeepCRE model

Firstly, we constructed the first patient level CRE datasets and established the initial DeepCRE model (Supplementary Fig. 1-3 and Supplementary Table 1). Upon identifying limitations the limitations of the initial DeepCRE model (details refer to Supplementary materials, Supplementary Fig. 4a,5), we turned to the architecture of domain separation network (DSN), which is a strategy for transfer learning and has been successfully applied in computer vision[20, 21, 22]. We propose the DeepCRE model zoo, comprising a suite of the DSN architecture (Fig. 2a) and its derivatives (Fig. 2b). The DeepCRE model zoo achieves an average performance increase of 17.21%, 11.52% and 7.69% over P-SDL models, C-MDL models and their combined counterparts, respectively (Supplementary Fig. 4b). Nonetheless, there remain four tumor types in which the DeepCRE model zoo demonstrates only average performance (Supplementary Fig. 5). Additionally, we observe no distinct differences in performance among these DeepCRE models (Supplementary Table 2). Since these models primarily differ in pretraining stages, we hypothesize that some pretraining settings may not be suitable for specific tumor types.

Diving deeper into the transferability difference of the pretraining data (details refer to Supplementary materials, Supplementary Fig. 6 and Supplementary Table 3,4), we propose a selective pretraining strategy for the patient unlabeled data. Contrary to the generic all-data pretraining method, our tumor type-adaptive pretraining strategy specifically aligns T2 patients (replace all patients) with all cell lines during the pretraining stage to enhance the accuracy of drug response predictions for T2 patients (Fig. 2c).

Employing this adaptive pretraining strategy significantly enhances the performance of our adv-loss-based DeepCRE models, contributing to the average performance increases of 3.51%, 4.92% and 11.28% for AE-adv, DSRN-adv and DSN-adv models, respectively (Fig. 2d and Supplementary Table 5). The DSN-adv model, in particular, stands out for its outstanding performance across various tumor types (Supplementary Fig. 7a and Supplementary Table 6). This leap in performance underscores the pivotal role of our pretraining strategy, especially in the alignment of cell line and patient gene expression profiles (GEPs). A comprehensive comparative analysis further detailing these pretraining strategies is available in the Supplementary materials (Supplementary Fig. 7b,c).

## DeepCRE demonstrates superior performance in patient level CRE across 13 tumor types

The DeepCRE models, benefiting from an enhanced pretraining strategy, exhibit SOTA performance across all tumor types, surpassing both P-SDL and C-MDL models (Fig.3a and Supplementary Table 6). On

average, DeepCRE models demonstrate performance improvements of 28.21%, 22.07% and 17.77% over P-SDL models, C-MDL models, and their combined counterparts, respectively (Supplementary Fig. 4c). Notably, the DSN-adv model emerges as a standout performer, achieving SOTA results in 12 out of 13 tumor types (Fig. 3a), and displaying average performance increases of 27.49%, 21.38% and 17.08% over P-SDL models, C-MDL models and their combined counterparts, respectively (Supplementary Fig. 4d). Generally, the AUROC performance of DeepCRE increases from the initial AE model to the DSN, DSN-mmd, and DSN-adv models.

To delve into the underlying mechanisms of this performance boost, we quantify the alignment effect (after pretraining) using two metrics: the relative maximum mean discrepancy[23] (MMD) and Kullback-Leibler (KL) divergence[24]. Both metrics demonstrate a decreasing trend from the original GEPs to the AE, DSN, DSN-mmd, and DSN-adv encoded embeddings, indicating enhanced alignment across these pretraining methods (Fig. 3b,c and Supplementary Table 7). Four tumor types exhibit a relative MMD of less than 0.3 for the DSN-adv model, as denoted by an asterisk (\*) in Fig. 3b, and are further elucidated in the t-SNE plots (Fig. 3d).

Furthermore, the DeepCRE DSN-adv model outperforms all of the P-SDL and C-MDL models across all tumor types (Fig. 3e). To explore the association between the model performance and paradigm selection, we compare the performance of DSN-adv with the best P-SDL and C-MDL models, respectively (Supplementary Fig. 8a and Supplementary Table 8). The percentage increase in performance of the DSN-adv model compared to the best P-SDL (brown) and C-MDL (blue) models illustrates the variability of pan-cancer improvement (Fig. 3f). The greatest increase for the best P-SDL model is observed in SARC, while the maximum increase for the best C-MDL model is seen in READ (Fig. 3f and Supplementary Fig. 8b). Notably, the tumor type COAD, which is associated with READ, also displays a substantial increase (Fig. 3f and Supplementary Fig. 8b). Intriguingly, a strong negative correlation ( $r = 0.782$ ) is observed between the drug overlap percentage and the log-scaled increase percentage for the P-SDL model (Supplementary Fig 8c,d and Supplementary Table 8). This suggests that the SDL paradigm, which lacks drug encodings, exhibits subpar performance when predicting unseen drugs[17]. In contrast, for the C-MDL mode, mutation-data-based methods generally outperform expression-data-based methods (Fig. 3g). We speculate that this is due to two reasons: i) transfer learning (alignment) is less crucial for mutation-based methods, as mutations primarily occur in tumor cells[25]; ii) transfer learning is essential for expression-based methods, as bulk expression data comprises not only tumor cells but also immune and stromal cells[26].

## DeepCRE’s potential in clinical pharmaceutical value assessment for pre-clinical drug candidates

To assess DeepCRE’s potential in clinical pharmaceutical value assessment for pre-clinical drug candidates, we have evaluated 233 small molecules across 13 tumor types (indications) and verified them through the DrugBank[27], ClinicalTrials[28], and Repurposing Hub[29] databases (Fig. 4a-c and Supplementary Fig. 9).

The pharmaceutical value assessment results are initially validated using the DrugBank database, which contains approved or investigational drugs with high confidence. Among the 17 small molecules listed in the DEI table, 10 drugs were recorded in DrugBank, while 7 small molecules lack any record (Fig. 4d and Supplementary Table 10). Visualized as a heatmap, the DEI table highlight predicted-efficient EDIs in purple (and DrugBank-recorded EDIs in blue), while predicted-inefficient EDIs are shaded grey (Fig. 4e). Notably, all DrugBank-recorded EDIs are predicted-efficient, indicating no false negatives. Furthermore, purple-colored EDIs represent "promising" opportunities for new drug development.

To further validate the predictions, we cross-reference in-clinical-test records from the ClinicalTrials database (Supplementary Table 11). Drug candidates identified by DeepCRE exhibit anti-tumor evidence in terms of mechanism of action (MoA) and current indications (Supplementary Fig. 10a,b). Nine drug candidates are in clinical testing, and after excluding widely-used Gemcitabine (Supplementary Fig. 10c,d), they are verified to be tested in various indications, including the 13 types of tumor indications used in our study (Fig. 6f and Supplementary Table 12). Mirroring the DrugBank analysis, the DEI table is visualized using



a heatmap, which also includes additional information about the tumor types in which the drug candidates were undergoing clinical testing (Fig. 6g). The predicted results demonstrate excellent agreement with the in-clinical-test records, indicating strong concordance between DeepCRE predictions and real-world clinical data (details refer to the Supplementary materials). Furthermore, five drug candidates are identified as Qualified drugs by DeepCRE (Fig. 6g), while no more than one Qualified drug candidate is discovered by any previous SOTA models (Supplementary Fig. 11). Additionally, the EDIs and Qualified drugs identified by our model are associated with 115 and 105 in-clinical-test records, respectively, representing substantial increases of 117% and 400%, respectively, compared to previous SOTA models (Fig. 6h,i). This result means the drug candidates discovered by our model show at least 5-fold increase in indication level CRE compared to any previous SOTA models.

Finally, we validate the DEI table through the Repurposing Hub database (Supplementary Fig. 12), which collects information on existing therapeutics repurposed for new disease indications from published papers[29]. Overall, the predictions from the DeepCRE are largely consistent with fully validated, in-clinical-test, and existing experimental evidence, indicating the strong alignment of our model with the expertise of real-world professionals in assessing the pharmaceutical value for pre-clinical drug candidates.

## **Validation of DeepCRE for efficient drug candidates identification in the CRC21 patient**

DeepCRE’s capability to identify efficient drug candidates is further validated in a clinical setting, focusing on the CRC21 patient. Despite receiving XEOLX treatment, the patient experience relapse after 13 days. Tumor samples collected prior to treatment are used to construct CRC organoids, enabling the evaluation of drug candidates identified by DeepCRE (Fig. 5a). This In-SMARchip drug testing methodology has been previously validated in lung and colorectal tumor organoids[30, 31]. The drug candidates are categorized into four sets based on their MoAs and the evaluation variance between DeepCRE and traditional methods (Fig. 5b,c). We try to keep the MoAs diversity in each drug set (Fig. 5b), and ensure the drug set with the largest evaluation disparity for comparison (Fig. 5c).

The drug testing results prove that DeepCRE outperforms traditional methods in two aspects. Firstly, six drug candidates (Set A) identified by DeepCRE exhibit significantly greater efficacy than a comparator set of two approved drugs (Set C), one of which is "Oxaliplatin combined with 5-Fluorouracil", the XEOLX treatment itself (Fig. 5d). Secondly, drug candidates with specific MoAs, such as PI3K/MTOR signaling and Chromatin histone acetylation, show potential to exceed traditional chemotherapy (e.g., drugs with the MoA of DNA replication) treatments (Fig. 5e).

## **Drug repurposing validation of DeepCRE in eight CRC organoids**

In order to further validate the potential of DeepCRE in drug repurposing for CRC, seven more CRC organoids are included for In-SMARchip drug testing. Among the eight CRC organoids tested, five exhibit a significant efficacy increase of set A over set C (Fig. 1d,e and Fig. 6a). Moreover, drug candidates in set A are also more efficient than two approved drugs in set C in the other three CRC organoids (Supplementary Fig. 13). Generally, the efficacy patterns of drug candidates were consistent across different patients, except for Sorafenib (D3), one of the receptor tyrosine kinase (RTK) inhibitors (Fig. 6b). However, there were variations in the exact correlation coefficients: inhibitors of PI3K/MTOR signaling and Chromatin histone acetylation show coefficients above 0.96, while those targeting DNA replication display coefficients ranging from 0.33 to 0.93, reflecting the diversity and complexity of chemotherapy[32, 33] (Fig. 3c).

Some intriguing insights emerge from the drug testing results, shedding light on the deeper mechanism exploration of drug candidates with similar MoAs. For instance, the DRC of GSK1059615 exhibits a significant increase at the highest concentration compared to other PI3K/MTOR inhibitors (Fig. 6d). Perturbation data from CMAP L1000[34] database provides some explanations (Fig. 6e-f). Cells treated with GSK1059615 show up-regulated cellular survival and stress response related pathways (isomerase activity, intramolecular transferase activity and phosphotransferases) and genes (IGFBP3, MYCBP, GTF2A2), DNA repair and

cytoskeleton regulation related genes (PARP1, RUVBL1, STAMPB), and down-regulated cell cycle checkpoints related pathways (protein tyrosine/MAP kinase/MAP kinase tyrosine phosphatase activity) and cell cycle related genes (STX1A, PARP6, KDM3A). The up-regulation and down-regulation of these genes and pathways may reflect the defensive mechanisms adopted by cells to resist the toxicity of high concentrations of drugs, potentially leading to the pausing of the cell cycle or the inhibition of cell death pathways[35, 36]. The other example is that the DRC of the drug Sorafenib, rather than another RTK inhibitor Dasatinib, declines at higher concentrations in three CRC organoids (Fig. 6g). It has been reported that some transport proteins may play a role in the accumulation and resistance of drugs, with Dasatinib being primarily restricted by ABCG1, and Sorafenib being mainly limited by ABCG2[37]. Further investigation suggests that ABCG2 expression, significantly lower in CRC tumor tissues compared to normal tissues[38] (Fig. 6h), may contribute to the reduced resistance of Sorafenib in CRC. Molecular docking analysis corroborates these findings, demonstrating a favorable binding affinity of Sorafenib to the target ABCG2 (Fig. 6i). Similar conclusions of binding poses and interactions have been drawn by a published paper, which presents single-particle cryo-EM studies of ABCG2 binding with another RTK inhibitor imatinib[39]. Furthermore, survival analysis reveals a negative correlation between ABCG2 expression and disease-free survival (DFS), implicating ABCG2-mediated multi-drug resistance (MDR) in CRC (Fig. 6j).

## References

- [1] Dolgin, E. The future of precision cancer therapy might be to try everything. *Nature* **626**, 470–473 (2024).
- [2] O’Dwyer, P. J. *et al.* The nci-match trial: lessons for precision oncology. *Nature Medicine* 1–9 (2023).
- [3] Wouters, O. J., McKee, M. & Luyten, J. Research and development costs of new drugs—reply. *JAMA* **324**, 518–518 (2020).
- [4] Sean. The process and costs of drug development (2022). <https://ftloscience.com/process-costs-drug-development> (2023).
- [5] Scannell, J. W., Blanckley, A., Boldon, H. & Warrington, B. Diagnosing the decline in pharmaceutical r&d efficiency. *Nature reviews Drug discovery* **11**, 191–200 (2012).
- [6] Ringel, M. S., Scannell, J. W., Baedeker, M. & Schulze, U. Breaking eroom’s law. *Nat Rev Drug Discov* **19**, 833–834 (2020).
- [7] Kornauth, C. *et al.* Functional precision medicine provides clinical benefit in advanced aggressive hematologic cancers and identifies exceptional responders. *Cancer discovery* **12**, 372–387 (2022).
- [8] Snijder, B. *et al.* Image-based ex-vivo drug screening for patients with aggressive haematological malignancies: interim results from a single-arm, open-label, pilot study. *The Lancet Haematology* **4**, e595–e606 (2017).
- [9] Luo, Y. *et al.* Toward unified ai drug discovery with multimodal knowledge. *Health Data Science* **4**, 0113 (2024).
- [10] Kuenzi, B. M. *et al.* Predicting drug response and synergy using a deep learning model of human cancer cells. *Cancer cell* **38**, 672–684 (2020).
- [11] Honkala, A., Malhotra, S. V., Kummar, S. & Junttila, M. R. Harnessing the predictive power of preclinical models for oncology drug development. *Nat. Rev. Drug Discovery* **21**, 99–114 (2022).
- [12] Vijayan, R., Kihlberg, J., Cross, J. B. & Poongavanam, V. Enhancing preclinical drug discovery with artificial intelligence. *Drug discovery today* **27**, 967–984 (2022).
- [13] Dincer, A. B., Janizek, J. D. & Lee, S.-I. Adversarial deconfounding autoencoder for learning robust gene expression embeddings. *Bioinformatics* **36**, i573–i582 (2020).
- [14] He, D., Liu, Q., Wu, Y. & Xie, L. A context-aware deconfounding autoencoder for robust prediction of personalized clinical drug response from cell-line compound screening. *Nat. Mach. Intell.* **4**, 879–892 (2022).
- [15] Cadow, J., Born, J., Manica, M., Oskoei, A. & Rodríguez Martínez, M. Pacmann: a web service for interpretable anticancer compound sensitivity prediction. *Nucleic Acids Res.* **48**, W502–W508 (2020).
- [16] Zhu, Y. *et al.* Tgsa: protein–protein association-based twin graph neural networks for drug response prediction with similarity augmentation. *Bioinformatics* **38**, 461–468 (2022).
- [17] Shen, B. *et al.* A systematic assessment of deep learning methods for drug response prediction: from in vitro to clinical applications. *Briefings Bioinf.* **24**, bbac605 (2023).
- [18] Kaitin, K. I. Deconstructing the drug development process: the new face of innovation. *Clinical Pharmacology & Therapeutics* **87**, 356–361 (2010).
- [19] Dickson, M. & Gagnon, J. P. The cost of new drug discovery and development. *Discovery medicine* **4**, 172–179 (2009).

- [20] Ganin, Y. *et al.* Domain-adversarial training of neural networks. *The journal of machine learning research* **17**, 2096–2030 (2016).
- [21] Bousmalis, K., Trigeorgis, G., Silberman, N., Krishnan, D. & Erhan, D. Domain separation networks. *Advances in neural information processing systems* **29** (2016).
- [22] Csurka, G. *et al.* *Domain adaptation in computer vision applications* (Springer, 2017).
- [23] Gretton, A., Borgwardt, K. M., Rasch, M. J., Scholkopf, B. & Smola, A. A kernel two-sample test. *The Journal of Machine Learning Research* **13**, 723–773 (2012).
- [24] Kullback, S. & Leibler, R. A. On information and sufficiency. *The annals of mathematical statistics* **22**, 79–86 (1951).
- [25] Martincorena, I. & Campbell, P. J. Somatic mutation in cancer and normal cells. *Science* **349**, 1483–1489 (2015).
- [26] Aran, D., Sirota, M. & Butte, A. J. Systematic pan-cancer analysis of tumour purity. *Nat. Commun.* **6**, 8971 (2015).
- [27] Wishart, D. S. *et al.* Drugbank 5.0: a major update to the drugbank database for 2018. *Nucleic Acids Res.* **46**, D1074–D1082 (2018).
- [28] Zarin, D. A., Tse, T., Williams, R. J., Califf, R. M. & Ide, N. C. The clinicaltrials.gov results database—update and key issues. *N. Engl. J. Med.* **364**, 852–860 (2011).
- [29] Corsello, S. M. *et al.* The drug repurposing hub: a next-generation drug library and information resource. *Nat. Med.* **23**, 405–408 (2017).
- [30] Hu, Y. *et al.* Lung cancer organoids analyzed on microwell arrays predict drug responses of patients within a week. *Nature Communications* **12**, 2581 (2021).
- [31] Wu, Y. *et al.* Grouped-seq for integrated phenotypic and transcriptomic screening of patient-derived tumor organoids. *Nucleic Acids Res.* **50**, e28–e28 (2022).
- [32] Alam, A. *et al.* Chemotherapy treatment and strategy schemes: A review. *Open Acc. J. of Toxicol* **2**, 555–600 (2018).
- [33] Makovec, T. Cisplatin and beyond: molecular mechanisms of action and drug resistance development in cancer chemotherapy. *Radiology and oncology* **53**, 148–158 (2019).
- [34] Subramanian, A. *et al.* A next generation connectivity map: L1000 platform and the first 1,000,000 profiles. *Cell* **171**, 1437–1452 (2017).
- [35] Copple, I. M., Goldring, C. E., Kitteringham, N. R. & Park, B. K. The keap1-nrf2 cellular defense pathway: mechanisms of regulation and role in protection against drug-induced toxicity. *Adverse Drug Reactions* 233–266 (2010).
- [36] Jones, T., Thor, H. & Orrenius, S. Cellular defense mechanisms against toxic substances. In *Toxic Interfaces of Neurons, Smoke and Genes: Proceeding of the European Society of Toxicology Meeting Held in Kuopio, June 16–19, 1985*, 259–271 (Springer, 1986).
- [37] Tang, S. C. *et al.* Impact of p-glycoprotein (abcb1) and breast cancer resistance protein (abcg2) gene dosage on plasma pharmacokinetics and brain accumulation of dasatinib, sorafenib, and sunitinib. *Journal of Pharmacology and Experimental Therapeutics* **346**, 486–494 (2013).
- [38] Liu, J. *et al.* An integrated tcga pan-cancer clinical data resource to drive high-quality survival outcome analytics. *Cell* **173**, 400–416 (2018).

- [39] Orlando, B. J. & Liao, M. Abcg2 transports anticancer drugs via a closed-to-open switch. *Nature communications* **11**, 2264 (2020).



**Figure 1: The objective and application of DeepCRE.**

**a**, Illustration of CRE distribution across different drug development stages, highlighting the potential benefits of in-silico CRE models in enhancing CRE availability during late-stage development. **b**, Comparative diagram showing the traditional vs. DeepCRE-assisted drug development processes. The DeepCRE-assisted method tends to increase success rates while reducing both time and costs. **c**, Conceptual framework of DeepCRE, aligning cell line and patient representations with the drug response space. This alignment enables the extrapolation of cell line drug responses to predict patient drug responses effectively. **d**, Heatmap displaying the Area Under the Curve (AUC) scores for 8 patient-derived colorectal cancer (CRC) organoids treated with four different sets of drugs. **e**, Boxplot illustrating the AUC scores of the four drug sets, with Set A (identified by DeepCRE) demonstrating significantly greater efficacy than Set C in 5/8 CRC organoids.

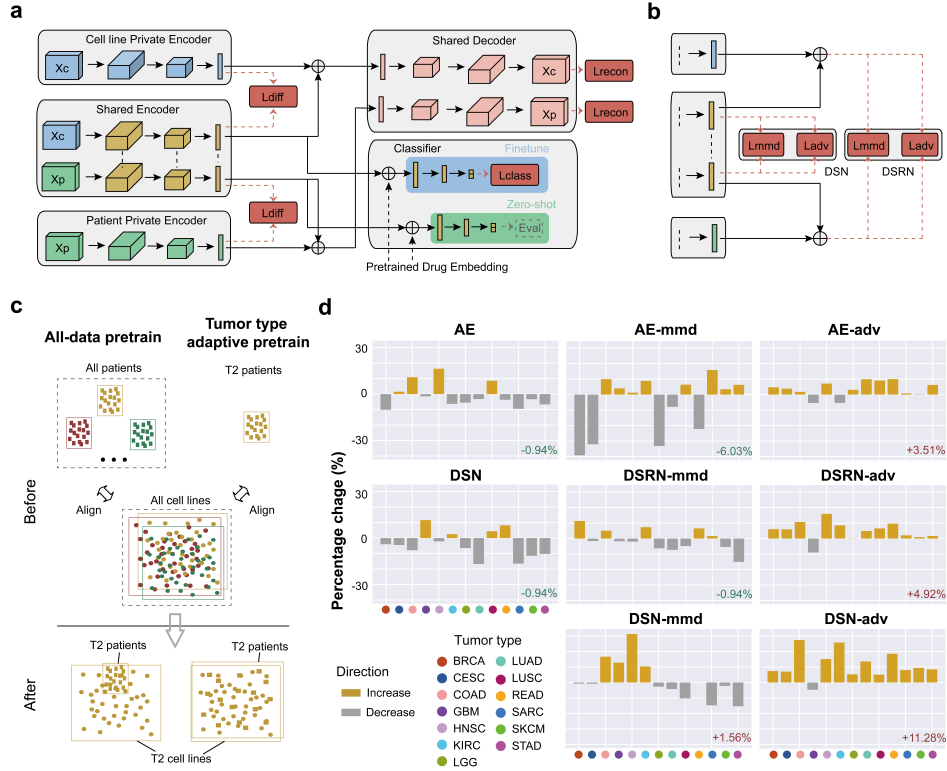


**Figure 2: The construction of the DeepCRE models.**

**a**, Illustration of DeepCRE: the representations of cell lines and patients are aligned using a domain separation network (DSN)[21] architecture. **b**, Variants of the DeepCRE model. In the DSN setting, the private embeddings of the source domain and target domain can be kept similar via optimizing  $L_{mmd}$  (DSN-mmd) or  $L_{adv}$  (DSN-adv). Moreover, another variation is that the concatenation of private and shared embeddings is kept similar, which can be represented as DSRN-mmd and DSRN-adv. **c**, Two pretraining strategies lead to different alignment of cell lines and patients of one specific tumor type. **d**, Bar plots showing the percentage change in performance from all-data pretraining to tumor type adaptive pretraining for eight DeepCRE models across 13 tumor types, with the numbers below representing the average percentage change among all tumor types. Three adv-loss-based DeepCRE models (the last column) generally improve significantly in 12 tumor types, except for GBM.

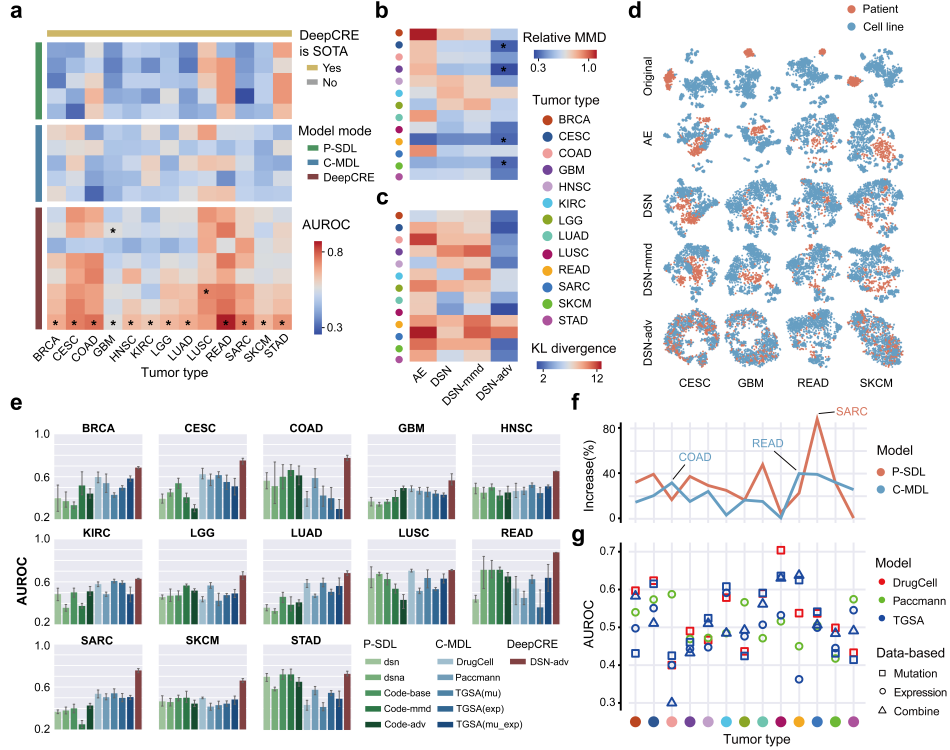


**Figure 3: DeepCRE outperforms other models in patient level CRE across 13 tumor types.**

**a**, Heatmap comparing the AUROC performance of P-SDL, C-MDL, and tumor type adaptive pretraining DeepCRE models. The listed models (from top to bottom) are P-SDL (dsn, dsna, Code-base, Code-mmd, Code-adv), C-MDL (DrugCell, Pacemmann, three types of TGSA) and DeepCRE (AE, DSN, AE-mmd, DSRN-mmd, DSN-mmd, AE-adv, DSRN-adv, DSN-adv) models. DeepCRE models achieve SOTA (marked with \*) performance in all tumor types. **b,c**, Heatmaps displaying alignment metrics for patients (brown) and cell lines (blue) across four pretraining methods: **b**, Maximum Mean Discrepancy[23] (MMD) relative to original expression within each tumor type. The relative MMD generally decreases from AE, DSN, DSN-mmd to DSN-adv, indicating improved alignment. Tumor types with relative MMD of DSN-adv less than 0.3 are marked with \* for further analysis in **d**. **c**, Kullback-Leibler (KL) divergence[24] also decreases from AE, DSN, DSN-mmd to DSN-adv. The KL divergence of original expression is not shown due to its nearly infinite value. **d**, t-SNE plots of gene expression encoded embeddings for four tumor types (marked with \* in **b**) from original expression to four DeepCRE models. Notably, DSN-adv (the last row) exhibits significant improvement in the alignment of patients and cell lines compared with other models. **e**, Bar plots indicating the AUROC performance of P-SDL, C-MDL and the DeepCRE DSN-adv model. DSN-adv outperforms all P-SDL and C-MDL models across all tumor types. **f**, Line chart showing the percentage increase in performance of the DSN-adv model compared with the best P-SDL (brown) and C-MDL (blue) models across all tumor types. The maximum increase for the best P-SDL model is observed in SARC, while the maximum increase for the best C-MDL model is seen in READ. The READ-related tumor type COAD also exhibits a substantial increase. **g**, Scatter plot indicating the AUROC performance of C-MDL models, with different shapes representing the types of used data. Generally, mutation-data-based methods outperform expression-data-based methods for C-MDL models.



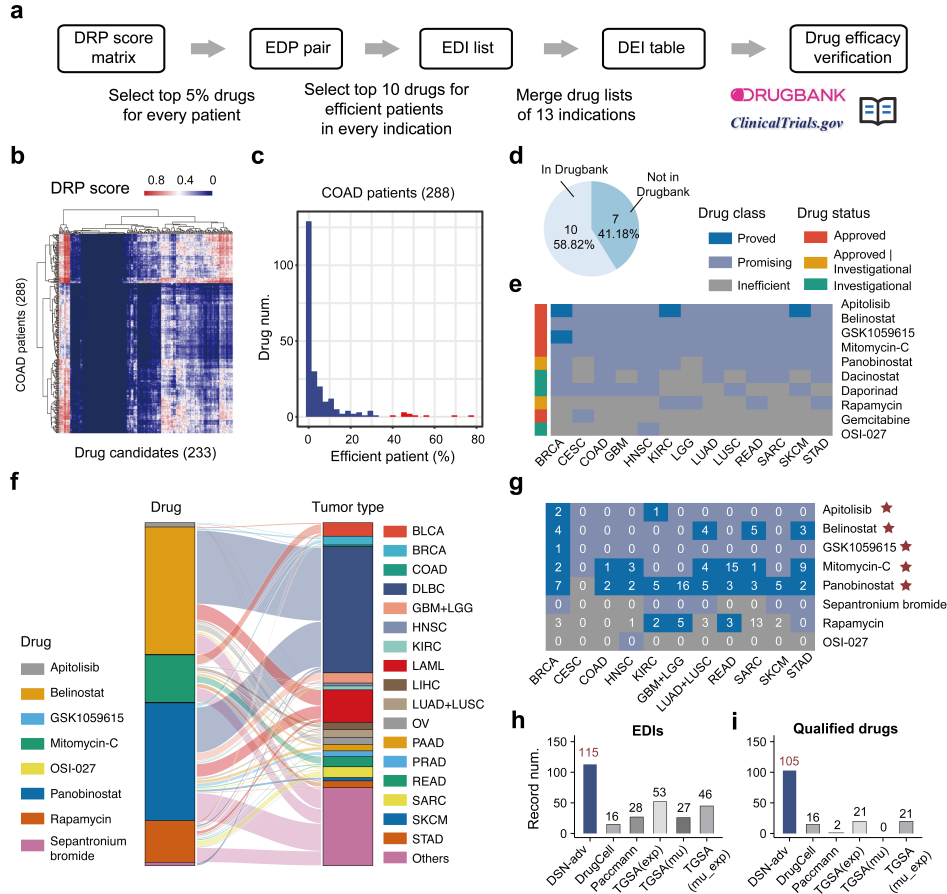


**Figure 4: DeepCRE outperforms other models in indication level CRE.**

**a**, Workflow illustrating the validation process of drug candidates discovered by DeepCRE. Refer to the Methods section for a detailed description. DRP: drug response for patients. EDP: efficient drugs for patients. EDI: efficient drugs for indications. DEI: drug efficacy for indications. **b**, Heatmap displaying DRP score matrix, e.g., COAD, comprising 288 patients (rows) and 233 drug candidates (columns). **c**, Histogram plot of EDPs for COAD. The top 10 drug candidates with the highest efficiency in patients are highlighted in red. Three drug candidates are efficient for over 50% of COAD patients. **d**, Pie chart demonstrating 10 out of 17 drug candidates have records in Drugbank. **e**, Heatmap of the DEI table. Both predicted-efficient and Drugbank-recorded EDIs are colored blue and labeled “Proved”. Only predicted-efficient EDIs are colored purple and labeled “Promising”. Predicted-inefficient EDIs are colored grey and labeled “Inefficient”. **f**, Sankey plot depicting the distribution of in-clinical-test tumor types for the drug candidates. **g**, Heatmap of the in-clinical-test records, colored by the combination of predicted results and in-clinical-test records. Qualified drugs are labeled with a pentagram. **h,i**, Bar plots demonstrating the record numbers of DSN-adv method and five C-MDL methods: **h** for EDIs, **i** for Qualified drugs.

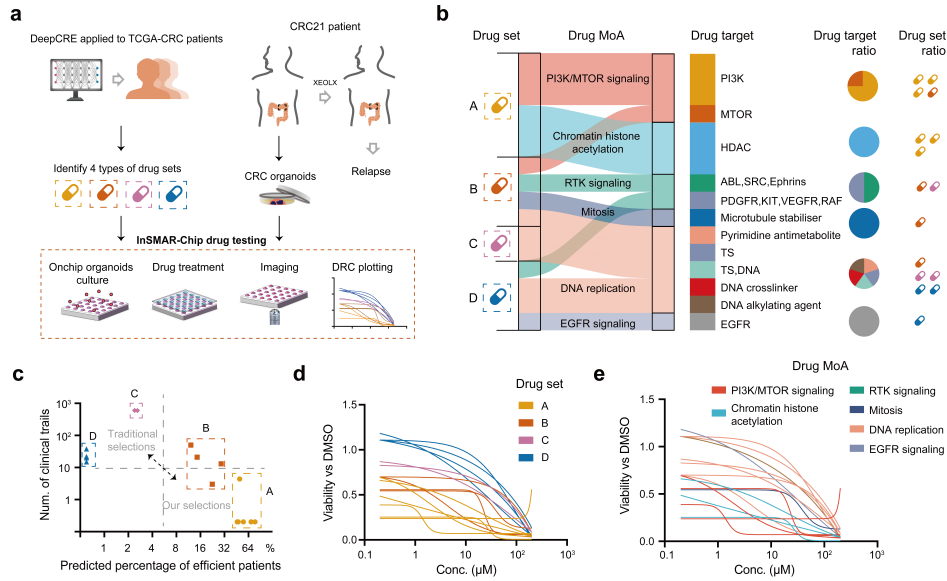


**Figure 5: Validation of DeepCRE for efficient drug identification in the CRC21 patient.**

**a**, Workflow demonstrating the utilization of DeepCRE to identify four types of drug sets, which were subsequently evaluated using CRC organoids derived from a patient who relapsed after traditional XEOLX treatment, employing InSMAR-Chip drug testing methodology. DRC: drug response curve. **b**, Sankey plot illustrating four drug sets with diverse mechanisms of actions (MoAs) and targets. **c**, 2D xy-plot displaying the evaluation outcomes of DeepCRE as well as traditional methods. **d**, DRC colored by the drug set indicating the ranking of drug efficacy: A>B>C>D. **e**, DRC colored by the drug MoA indicating that certain drugs with specific MoAs exhibit relatively greater efficacy, such as PI3K/MTOR signaling and Chromatin histone acetylation.

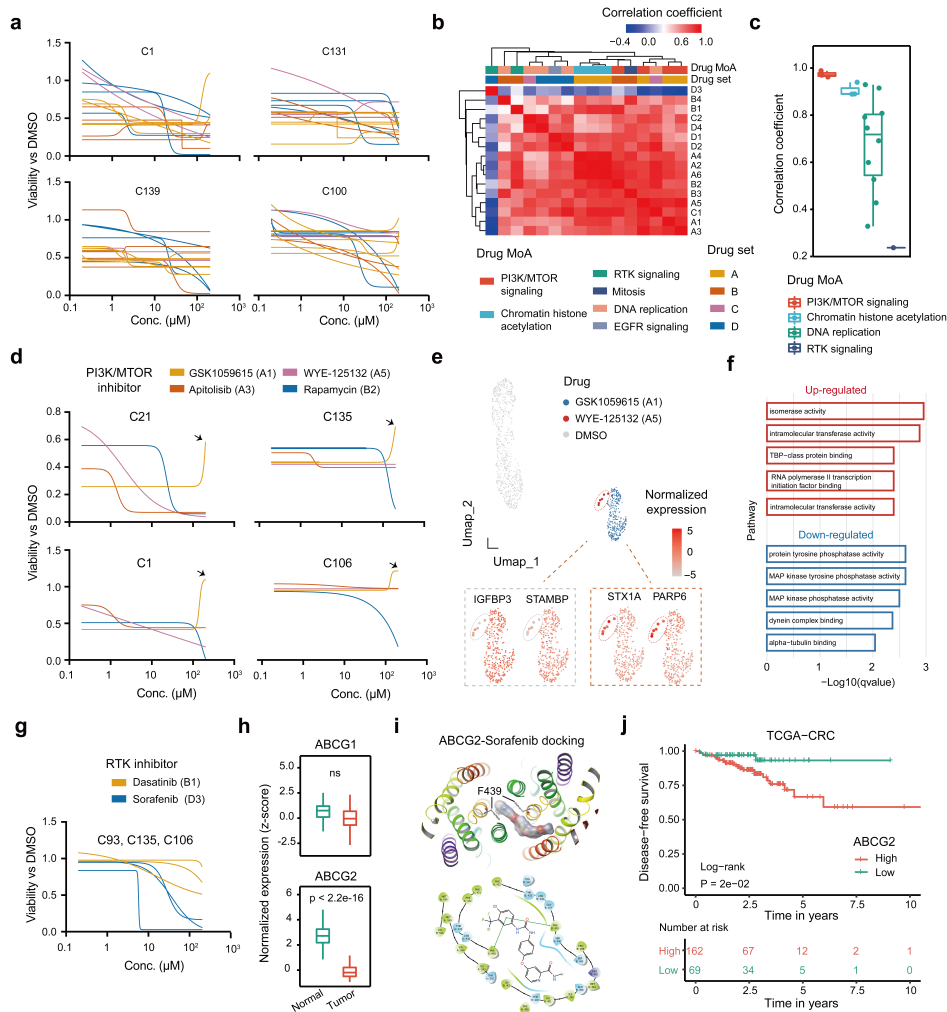


**Figure 6: Drug repurposing validation of DeepCRE in eight CRC organoids.**

**a**, DRC across four CRC organoids, colored by the drug set, indicating that the drug set A possesses significantly greater effectiveness than drug set C. **b**, Heatmap of correlation coefficients of drugs, demonstrating that the drug efficacy is related to the drug MoA and the drug set. **c**, Boxplot of correlation coefficients of drugs, indicating differences in the distribution of efficient populations among drugs targeting DNA replication. **d**, DRC of PI3K/MTOR inhibitor drugs across four CRC organoids, showing the dramatic increase in DRC of the drug GSK1059615 at the highest concentration. **e**, Umap plot of gene expression of cells after different perturbations, with representative differential genes shown in the dashed frame. **f**, Bar plot of enriched pathways, with up-regulated pathways colored in red and down-regulated pathways in blue. **g**, DRC of RTK inhibitor drugs across three CRC organoids, showing the decline in DRC of the drug Dasatinib, rather than Sorafenib, at higher concentrations. **h**, Boxplot of genes ABCG1 and ABCG2 in the TCGA-CRC cohort, indicating significantly lower expression of ABCG2 in tumor samples. **i**, 3D and 2D diagram of ABCG2-Sorafenib docking. **j**, Survival curve of ABCG2 in the disease-free survival (DFS) of TCGA-CRC cohort.